Influence of the cluster's size of random gold nanostructures on the fluorescence of single CdSe–CdS nanocrystals

Damien Canneson, Stéphanie Buil, Xavier Quélin, Clémentine Javaux, Benoît Dubertret, J.-P Hermier

Gold Bull (2013) 46:329–334
DOI 10.1007/s13404-013-0123-8

ORIGINAL PAPER

Influence of the cluster's size of random gold nanostructures on the fluorescence of single CdSe–CdS nanocrystals

Damien Canneson · Stéphanie Buil · Xavier Quélin · Clémentine Javaux · Benoît Dubertret · Jean-Pierre Hermier

Published online: 29 November 2013

Abstract It is well known that coupling a single emitter to metallic structures modifies drastically its fluorescence properties compared to single emitter in vacuum. Depending on various parameters such as the nature of the metal or the geometry of the metallic structure, quenching or intensity enhancement as well as radiative processes acceleration are obtained through the creation of new desexcitation channels. The use of metallic random structures gives the opportunity to magnify the effect of the coupling by strongly confined electromagnetic fields. A gold film at the percolation threshold is an interesting illustration of that effect. Here, we study the influence of the method used to realize these films through two different examples. First, we show that the mean size of the gold clusters constituting the film depends on the deposition method. Even if similar optical properties (in particular far-field absorption) are exhibited by the structures, crucial differences appear in the fluorescence of single emitters when coupled to the two kinds of random gold film. Especially, we focus our attention on the creation of desexcitation channels and show that they are cluster size dependent.

Keywords Nanocrystals · Metallic random structures · Surface plasmon resonances · Purcell effect

D. Canneson · S. Buil · X. Quélin (✉) · J.-P. Hermier
Groupe d'Étude de la Matière Condensée,
Université de Versailles-Saint-Quentin-en-Yvelines,
CNRS UMR8635, 45 avenue des États-Unis,
78035 Versailles, France
e-mail: quelin@physique.uvsq.fr

J.-P. Hermier
e-mail: jean-pierre.hermier@uvsq.fr

C. Javaux · B. Dubertret
Laboratoire de Physique et d'Étude des Matériaux,
CNRS UMR8213, ESPCI, 10 rue Vauquelin,
75005 Paris, France

J.-P. Hermier
Institut Universitaire de France, 103 boulevard
Saint-Michel, 75005 Paris, France

Introduction

Colloidal core–shell nanocrystals (NCs) are promising single emitters. They are synthesized in solution and so are easy to use and to prepare at low cost. They are bright (high quantum yield (QY)) and photostable at room temperature, opening a wide variety of applications, such as quantum optics [1], biomedical applications [2, 3], or optoelectronics [4–6]. But for an optimal use of NCs, a fine tailoring of their fluorescence properties is needed.

It is well known [7] that the control of the fluorescence properties, such as polarization, emission diagram, or photoluminescence (PL) decay, can be achieved by modifying the electromagnetic (EM) surroundings of the emitter. For example, the modification of the PL decay can be achieved by the use of cavities. In the weak coupling regime, the modification of the PL decay can be quantified through the Purcell factor $\left(F_P = \frac{\tau_0}{\tau}\right)$ [8], where $\frac{1}{\tau_0}$ and $\frac{1}{\tau}$ are the decay rates of the emitter in free space and in the cavity, respectively.

Specific dielectric structures have been investigated, such as micro-disks [9], micro-pillars [10, 11], or other microcavities [12]. Dielectric cavities with very high quality factors (Q) can be designed and Purcell factors (F_P) greater than 10 have been obtained. In these cavities, F_P is proportional to the ratio $\frac{Q}{V}$, where V is the modal volume in the cavity. It is obvious that increasing F_P can be obtained

either by increasing Q or decreasing V. The reduction of V is limited by the diffraction: it is not possible to obtain, in cavities, smaller modal volume than the cube of the wavelength. Then, increasing Q is the key to achieve high F_P. But this is meaningful only if the bandwidth of the emitter is narrower than Q. Otherwise, in the F_P expression, Q is replaced by the bandwidth of the emitter. This is a strong limitation for controlling the emitter's emission with dielectric cavities at room temperature, where emitters usually exhibit a large bandwidth.

Since the results obtained by Drexhage et al. [13], it is known that metallic structures can also be used to modify the fluorescence properties of an emitter. Two major advantages of the metallic structures are due to plasmon resonances: strong localizations of EM field and wide bandwidths. Thanks to the strong localization of the EM field, modal volumes smaller than the cube of the wavelength can easily be obtained and thanks to the spectral width of the plasmon resonances, it is possible to couple efficiently large bandwidth emitters or different kind of emitters to the same metallic structure.

However, a strong drawback of the metallic films is losses. Some metallic structures [14, 15] have been specifically designed to redirect the non-radiative plasmons. The parameters involved in these studies are the size of the metallic nanostructure and its distance and orientation with respect to the emitter [16, 17]. In these kind of studies, mastering the relative position of the emitter to the metallic cluster plays a crucial role. In this paper, we propose to use random gold films, allowing us to skirt this major difficulty. These random gold films have many advantages for the coupling with the fluorescence of the emitter. Due to a large number of plasmon resonances, the coupling can be efficient whatever the emission wavelength is. A wide variety of plasmons is also observed on these films, including radiative ones that can induce an efficient collection of the fluorescence. It will be shown in this article that randomness is not the only parameter controlling the coupling between emitters and metallic structures. The size of the random metallic clusters also plays a great role in the modification of the fluorescence properties.

Samples and experimental setup

The random gold structures were elaborated using two different methods: thermal evaporation under ultrahigh vacuum (10^{-9} torr, method 1) and radio frequency sputtering (method 2). For both methods, the films were obtained on the same kind of substrate and below the percolation threshold. In this concentration regime, the deposited layer exhibit a wide variety, in shapes and sizes, of unconnected gold clusters.

The local structure of the gold films was observed with an Atomic Force Microscope (AFM, Dimension 3100, Bruker AXS). Their optical properties (transmission, reflection, and absorption) were studied with a Perking Elmer LAMBDA 950 spectrophotometer.

The NCs have been synthesized following the method described in [18]. They are core–thick shell CdSe–CdS NCs, with a 5-nm-diameter core and a 10-nm-thick shell. The fluorescence emission is around 660 nm with a full width at half maximum of 30 nm.

The fluorescence of the NCs was analyzed with an inverted confocal microscope (IX 71, Olympus). The excitation was performed with a pulsed diode laser (LDH 485, PicoQuant, pulse duration $\sim$ 100 ps) emitting at 485 nm, with a repetition rate of 2.5 MHz for NCs deposited on glass coverslip (reference) and 40 MHz for NCs deposited on the gold films.

The fluorescence was collected through an air objective with numerical aperture (NA) of 0.95. An oil objective with NA of 1.4 was also used for the characterization on glass coverslip.

The optical signal is sent in a high-sensitivity Hanbury-Brown and Twiss (HB-T) setup (avalanche photodiodes PDM series, MPD, time resolution 50 ps). The signal is recorded by a PicoHarp 300 module (PicoQuant, time resolution 64 ps). For each experiment, the absolute time of arrival of the photons with close to 100 ps accuracy is given. Then the time evolution of the intensity, the correlation between photon pairs, and the PL decay are extracted.

The CdSe–CdS nanocrystals

Unlike usual CdSe–ZnS NCs, for which it is impossible to grow a thick shell without defects, CdSe–CdS NCs can have shells as thick as 15 nm. Due to relative positions of the conduction and valence bands at the interface between CdSe and CdS, when an electron-hole (e-h) pair is created, the electron is delocalized in the whole structure of the nanocrystal while the hole remains confined in the core. This affects the fluorescence lifetime, increasing from $\sim$ 20 ns for CdSe–ZnS NCs to $\sim$ 70 ns for CdSe–CdS NCs. The blinking phenomenon, which is the main drawback of CdSe–ZnS NCs and consists on non-emitting periods due to ionization and Auger effect [19], is strongly reduced. More precisely, the ionized state of CdSe–CdS NCs is still a radiative state but with a reduced efficiency. The duration of the ionization periods does not exceed tens of milliseconds [20]. The thick shell also plays the role of a spacer. It prevents the

quenching due to non-radiative processes occurring close to a metallic surface. Depositing directly these thick-shell NCs on gold films is then possible [21].

Typical fluorescence properties are depicted on Fig. 1. The record of the intensity versus time (Fig. 1a) shows the fluctuations of the intensity. The histogram of this trace exhibits a maximum value with a tail due to the remaining flickering. The most probable value will be used to compare intensities on gold films.

The PL decay is shown on Fig. 1b and is well fitted by a bi-exponential decay curve. The longest time decay of the bi-exponential corresponds to the neutral state of the NC and the shortest one is due to the ionized state of the NC. Details can be found in [22].

NCs were excited in the low power excitation regime (10 % of the saturation regime). In this regime, the probability to create e-h pairs is described by a Poisson statistics [20], and 90 % of the pulses will not generate an e-h pair, 9.5 % will generate one e-h pair, and only 0.5 % will generate more than one e-h pair. The fraction of multi-excitons is small enough to be neglected for future intensity comparisons.

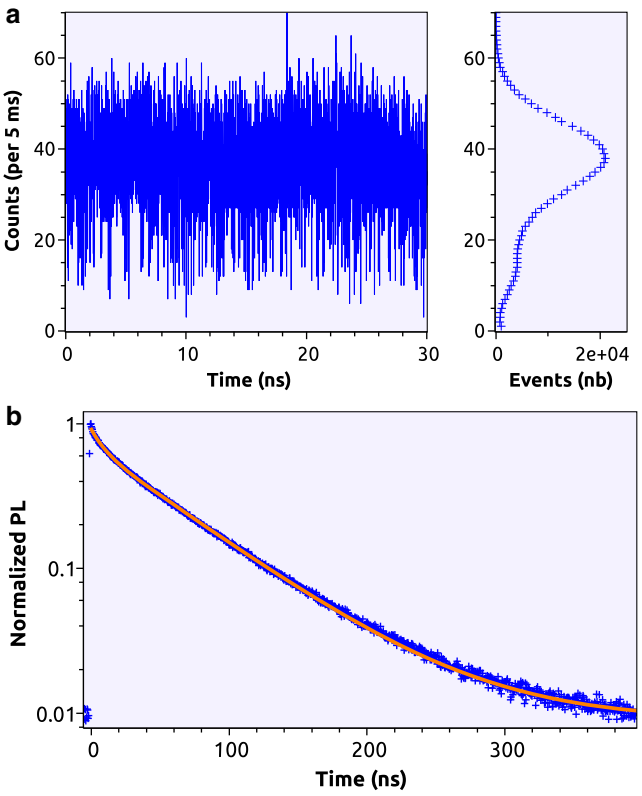

Fig. 1 Properties of the fluorescence of a single NC on reference substrate (glass coverslip): **a** intensity versus time of the fluorescence and its histogram, and **b** PL decay, fitted by a bi-exponential decay curve ($\tau_{slow} = 70$ ns, $\tau_{fast} = 15$ ns)

The gold structures

The two methods used to elaborate the gold films lead to structures with similarities and differences which can be observed through the local structure and the far-field spectrum (Fig. 2). The topographic images (Fig. 2a, b) show a similar general structure of the films, i.e., non-connected random clusters of widely different shapes, but either the mean lateral dimensions or the height of the clusters are smaller, roughly by a factor two, for the films elaborated by method 2 (Fig. 2b) compared to those elaborated by method 1 (Fig. 2a). The mass thickness (~ 7.5 nm) is very close for the two films. Despite the difference in size of the clusters, the same quantity of metal is deposited on the films. To the end of the study, the structures elaborated by method 1 will be called *big* structures and the structures elaborated by method 2 will be called *small* structures.

Far-field optical spectrum are depicted on Figs. 2c, d. The general behavior of absorption, reflection, and transmission are nearly the same. The values of the reflection and the transmission are slightly different, but the absorption is the same for both structures with a plateau covering a part of the visible and extending to the infrared. This plateau corresponds to a wide range of plasmon resonances due to the distribution of metallic cluster sizes and shapes.

To evaluate the disorder, it is common to calculate the fractality of the perimeter of the clusters [23]. The perimeter P_c of a cluster is said to be fractal when $P_c \propto S^{\frac{D}{2}}$, where S is the surface of the cluster and D, the fractal dimension, is a non-integer number. Here, for the big structures, $D = 1.88$. For the small ones, $D \simeq 1.9$. For the two films, D is nearly the same and very close to the well-known Hausdorff value for these kinds of structure [23].

Due to the disorder of these metallic structures, strong localizations and enhancements of the EM fields have been observed [24]. These localizations of energy are usually called *hot spots*. Their position, number, and intensity depend on the excitation parameters. The higher the wavelength, the stronger the enhancement and localization.

Coupling NCs to the gold structures

NCs are directly deposited on the gold nanostructures without any spacer. Only their fluorescence is coupled to the plasmon resonances, but not the excitation laser which is outside the absorption plateau. The main modification induced by the coupling between plasmons and NCs emission is a strong acceleration of the fluorescence decay (Fig. 3a). Due to this strong acceleration, the lifetime of the ionized state becomes too short to be correctly extracted with our setup. Consequently, we only focus on the modifications of the neutral state's lifetime. The acceleration is

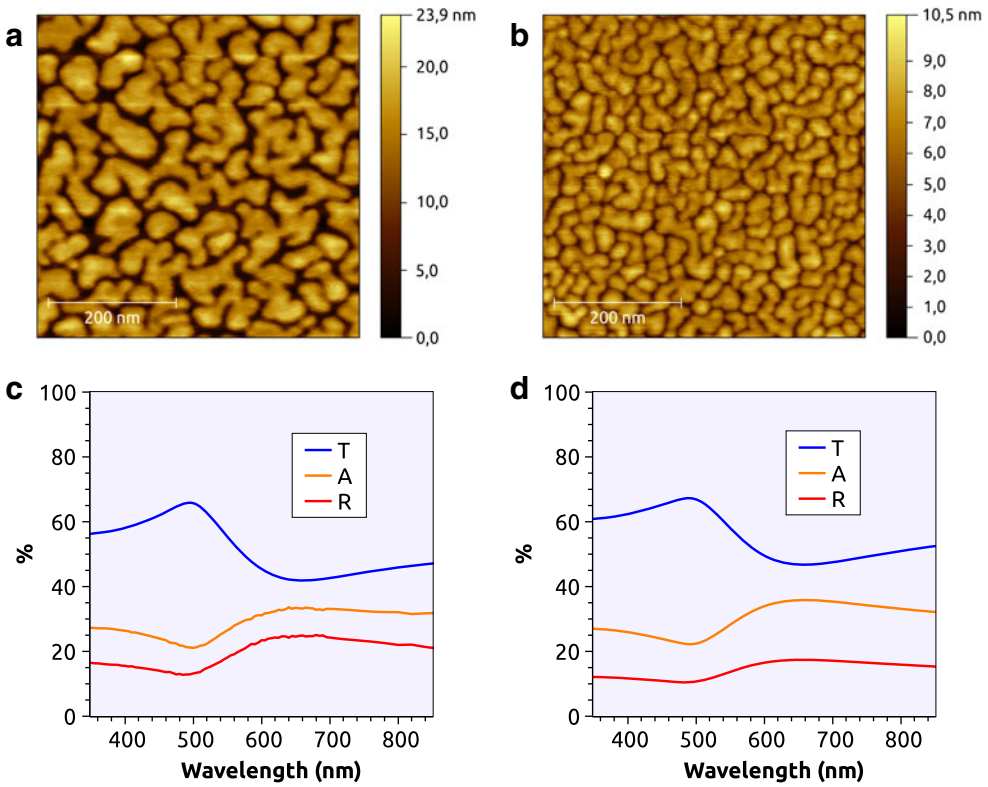

Fig. 2 AFM topography (**a**, **b**) and far-field spectra (**c**, **d**) of the random gold structures deposited by thermal evaporation under ultrahigh vacuum (**a**, **c**) and radio frequency sputtering (**b**, **d**)

due to the opening of new desexcitation channels that can be radiative or non-radiative. The intensity of the fluorescence is then strongly modified. Figure 3a shows these modifications on both structures, where the intensity is plotted versus F_P for a large set of NCs.

On Fig. 3a, a strong increase of the decay rate is observed. For each set of data, the range of F_P values is wide, with a factor of 10 between the less and the most accelerated NCs. For the big structures, F_P ranges from 6 to 60. For the small structures, F_P ranges from 12 to 120. This wide distribution is attributed to the random distribution of positions and intensities of the *hot spots* on the surface of the film. Comparing the two sets of data, it is clear that the emission is more accelerated on the small structures: the F_P distribution is centered on higher values on the small structures than on the big ones but with a comparable width.

The strong modification of the collected fluorescence intensity is observed on Fig. 3a. The intensity of fluorescence collected by the setup for NCs on gold structures is normalized by the intensity collected on glass coverslip. The different repetition rates of the laser used in both cases has been taken into account. The intensity is far lower on

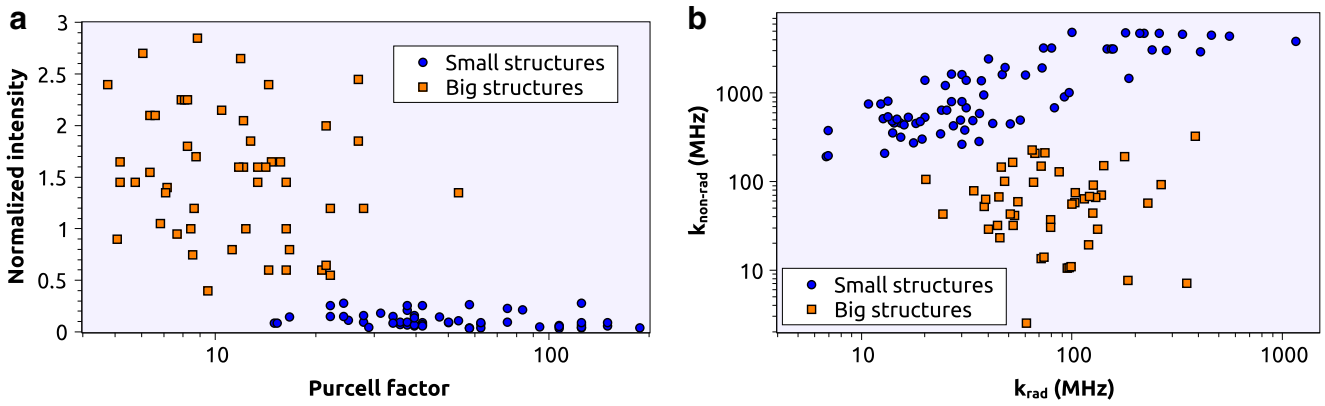

Fig. 3 Modification of the single NCs fluorescence properties due to the coupling with the gold films: **a** the normalized intensity $\left(\frac{I}{I_{glass}}\right)$ versus the Purcell factor $\left(\frac{\tau_0}{\tau}\right)$ for NCs deposited on big (*orange squares*) and small (*blue circles*) structures and **b** radiative against non-radiative decay rates both for the coupling on big (*orange squares*) and small (*blue circles*) structures

small structures and the ratio of signal-to-noise is too low to keep the same excitation power than on big structures. A higher excitation, still remaining in a low power excitation regime, has been needed but intensity results have been renormalized. A wide range of intensities can be obtained, up to three times and down to 0.05 times the reference intensity on glass coverslip. Here again, this distribution is due to the wide variety of plasmons existing on this type of structures. The intensities are clearly higher for the big structures, with values ranging from 0.4 to 2.9 times the reference on glass coverslip. For the small structures, most of the fluorescence is lost in non-radiative channels as the intensity is always lower than 0.4 times that on the glass coverslip.

A common set of F_P values can be found on both structures, from 12 to 60, but even for this set, intensities are far lower on small structures. This means that the desexcitation channels on the two structures are completely different. The number of non-radiative channels is more important on the small structures. The calculation of the number of radiative and non-radiative channels is done as follows. First, we select the intensity corresponding to the neutral state, giving us F_{coll}. Then, we extract the fluorescence lifetime, giving us the total decay rate $\tau = \frac{1}{k_{\text{tot}}}$. Using the two well-known equations

$$k_{\text{tot}} = k_{\text{rad}} + k_{\text{non-rad}}$$

and

$$F_{\text{coll}} = \frac{k_{\text{rad}}}{k_{\text{rad}} + k_{\text{non-rad}}},$$

we can deduce the values of k_{rad} and $k_{\text{non-rad}}$, respectively (details can be found in [25]). This procedure has been applied on the experimental data, and the results are plotted on Fig. 3b.

A wide range of radiative and non-radiative decay rates is obtained. For both structures, the range of radiative decay rates is nearly the same, slightly wider for the small structures. The radiative channels are comparable on both structures. On the contrary, the value of the non-radiative decay rate is always higher for the small structures. The distribution is still wide, clearly higher for small structures. Non-radiative channels are much more likely than radiative ones. This explains the data shown on Fig. 3a. For the small structures, desexcitation is mostly due to non-radiative processes. The acceleration of PL decay is higher on small structures due to a higher total number of decay channels. Then, higher F_Ps on the small structures correspond to lower intensities.

The size of the initial clusters seems to play a crucial role. This could be in agreement with results obtained for the coupling of single emitter with gold nanospheres [26]. The smallest is the sphere, the strongest is the coupling, but also the lowest is the collection. Nevertheless, one has to bear in mind that the metallic structures studied in this article are much more complex than single nanoparticles. For a more complete understanding, one has to take into account the distance between the clusters, the fact that the emitter interacts with many of them and the roughness of the film [27]. The influence of long range interaction processes might also be considered.

However, our results could explain crucial differences obtained by several groups concerning the coupling of single emitters with random structures [28–30]: it strongly depends on the size of the gold clusters and the method used to obtain the random gold films.

Conclusion

All the above results show that the desexcitation channels are really different on both structures even if the two films are at the vicinity of the percolation threshold. A higher number of desexcitation channels are present on the small structures, but they are mainly non-radiative. It results in strongly accelerated decay processes with very low collected intensity. Fastening the desexcitation processes on small structures is mainly due to non-radiative processes. On the contrary, on the big structures, the total number of desexcitation channels is lower, but the ratio between radiative and non-radiative ones is more balanced. The radiative processes are slightly less accelerated, but the collection of the fluorescence intensity is far higher. The coupling then realizes a compromise between the fastening of recombination process and the collection efficiency. Our results finally show that the coupling between a single emitter and a random gold film near the percolation threshold depends strongly on the microscopic structure of the film, both in terms of Purcell effect and far-field emission.

Acknowledgments This work has been supported by the Region Ile-de-France in the framework of du DIM “des atomes froids aux nanosciences” by Agence Nationale de la Recherche (under grants QDOTICS ANR-12-BS-008), and by the Institut Universitaire de France.

References

1. Brokmann X, Messin G, Desbiolles P, Giacobino E, Dahan M, Hermier J-P (2004) Colloidal CdSe/ZnS quantum dots as single-photon sources. New J Phys 6:99. doi:10.1088/1367-2630/6/1/099
2. Michalet X, Pinaud FF, Bentolila LA, Tsay JM, Doose S, Li JJ, Sundaresan G, Wu AM, Gambhir SS, Weiss S (2005) Quantum dots for live cells, in vivo imaging, and diagnostics. Science 307:538–544. doi:10.1126/science.1104274
3. Tomczak N, Jańczewski D, Dorokhin D, Han M-Y, Vancso G J (2012) Enabling biomedical research with designer quantum dots. Nanotechnol Regen Med, Methods Mol Biol 811:245–265. doi:10.1007/978-1-61779-388-2_16

4. Talapin DV, Lee JS, Kovalenko MV, Shevchenko EV (2010) Prospects of colloidal nanocrystals for electronic and optoelectronic applications. Chem Rev 110:389–458. doi:10.1021/cr900137k
5. Sargent EH (2012) Colloidal quantum dot solar cells. Nat Photonics 6:133–135. doi:10.1038/nphoton.2012.33
6. Shirasaki Y, Supran GJ, Bawendi MG, Bulović V (2013) Emergence of colloidal quantum-dot light-emitting technologies. Nat Photonics 7:13–23. doi:10.1038/nphoton.2012.328
7. Lakowicz JR (2006) Principles of fluorescence spectroscopy. Springer, New York
8. Purcell EM (1946) Spontaneous emission probabilities at radio frequencies. Phys Rev 69:681. doi:10.1103/PhysRev.69.674.2
9. Gayral B, Gérard JM, Sermage B, Lemaître A, Dupuis C (2001) Time-resolved probing of the Purcell effect for InAs quantum boxes in GaAs microdisks. Appl Phys Lett 78:2828. doi:10.1063/1.1370123
10. Gérard JM, Sermage B, Gayral B, Legrand B, Costard E, Thierry-Mieg V (1998) Enhanced spontaneous emission by quantum boxes in a monolithic optical microcavity. Phys Rev Lett 81:1110–1113. doi:10.1103/PhysRevLett.81.1110
11. Kahl M, Thomay T, Kohnle V, Beha K, Merlein J, Hagner M, Halm A, Ziegler J, Nann T, Fedutik Y, Woggon U, Artemyev M, Pérez-Willard F, Leitenstorfer A, Bratschitsch R (2007) Colloidal quantum dots in all-dielectric high-Q pillar microcavities. Nano Lett 7:2897–2900. doi:10.1021/nl071812x
12. Goldberg D, Menon VM (2013) Enhanced amplified spontaneous emission from colloidal quantum dots in all-dielectric monolithic microcavities. Appl Phys Lett 102(081119). doi:10.1063/1.4793753
13. Drexhage KH, Kuhn H, Schäfer FP (1968) Variation of the fluorescence decay time of a molecule in front of a mirror. Ber Bunsenges Phys Chem 72:329. doi:10.1002/bbpc.19680720261
14. Song J-H, Atay T, Shi S, Urabe H, Nurmikko AV (2005) Large enhancement of fluorescence efficiency from CdSe/ZnS quantum dots induced by resonant coupling to spatially controlled surface plasmons. Nano Lett 5:1557–1561. doi:10.1021/nl050813r
15. Belacel C, Habert B, Bigourdan F, Marquier F, Hugonin J-P, Michaelis de Vasconcellos S, Lafosse X, Coolen L, Schwob C, Javaux C, Dubertret B, Greffet J-J, Senellart P, Maitre A (2013) Controlling spontaneous emission with plasmonic optical patch antennas. Nano Lett 13:1516–1521. doi:10.1021/nl3046602
16. Pfeiffer M, Lindfors K, Wolpert C, Atkinson P, Benyoucef M, Rastelli A, Schmidt OG, Giessen H, Lippitz M (2010) Enhancing the optical excitation efficiency of a single self-assembled quantum dot with a plasmonic nanoantenna. Nano Lett 10:4555–4558. doi:10.1021/nl102548t
17. Manjavacas A, García de Abajo F J, Nordlande P (2011) Quantum plexcitonics: strongly interacting plasmons and excitons. Nano Lett 11:2318–2323. doi:10.1021/nl200579f
18. Mahler B, Spinicelli P, Buil S, Quélin X, Hermier J-P, Dubertret B (2008) Towards non-blinking colloidal quantum dots. Nat. Mater 7:659–664. doi:10.1038/nmat2222
19. Efros AL, Rosen M (1997) Random telegraph signal in the photoluminescence intensity of a single quantum dot. Phys Rev Lett 78:1110–1113. doi:10.1103/PhysRevLett.78.1110
20. Spinicelli P, Buil S, Quélin X, Mahler B, Dubertret B, Hermier J-P (2009) Bright and grey states in CdSe–CdS nanocrystals exhibiting strongly reduced blinking. Phys Rev Lett 102(136801). doi:10.1103/PhysRevLett.102.136801
21. Canneson D, Mallek-Zouari I, Buil S, Quélin X, Javaux C, Mahler B, Dubertret B, Hermier J-P (2011) Strong Purcell effect observed in single thick-shell CdSe/CdS nanocrystals coupled to localized surface plasmons. Phys Rev B 84(245423). doi:10.1103/PhysRevB.84.245423
22. Javaux C, Mahler B, Dubertret B, Shabaev A, Rodina AV, Efros AL, Yakovlev DR, Liu F, Bayer M, Camps G, Biadala L, Buil S, Quélin X, Hermier J-P (2013) Thermal activation of non-radiative Auger recombination in charged colloidal nanocrystals. Nat Nano 8:206–212. doi:10.1038/nnano.2012.260
23. Mandelbrot B (1983) The fractal geometry of nature. Freeman, New York
24. Buil S, Aubineau J, Laverdant J, Quélin X (2006) Local field intensity enhancements on gold semicontinuous films investigated with an aperture nearfield optical microscope in collection mode. J Appl Phys 100(063530). doi:10.1063/1.2335664
25. Brokmann X, Coolen L, Hermier J-P, Dahan M (2005) Emission properties of single CdSe/ZnS quantum dots close to a dielectric interface. Chem Phys 318:91. doi:10.1016/j.chemphys.2005.06.032
26. Mertens H, Koenderink AK, Polman A (2007) Plasmon-enhanced luminescence near noble-metal nanospheres: comparison of exact theory and an improved Gersten and Nitzan model. Phys Rev B 76(115123). doi:10.1103/PhysRevB.76.115123
27. Biehs S-A, Greffet J-J (2011) Statistical properties of spontaneous emission from atoms near a rough surface. Phys Rev A 84(052902). doi:10.1103/PhysRevA.84.052902
28. Cazé A, Pierrat R, Carminati R (2012) Radiative and non-radiative local density of states on disordered plasmonic films. Photonics Nanostruct Fundam Appl 10:339–344. doi:10.1016/j.photonics.2012.03.001
29. Canneson D, Mallek-Zouari I, Buil S, Quélin X, Javaux C, Dubertret B, Hermier J-P (2012) Enhancing the fluorescence of individual thick shell CdSe/CdS nanocrystals by coupling to gold structures. New J Phys 14(063035). doi:10.1088/1367-2630/14/6/063035
30. Shimizu KT, Woo WK, Fisher BR, Eisler HJ, Bawendi MG (2002) Surface-enhanced emission from single semiconductor nanocrystals. Phys Rev Lett 89(117401). doi:10.1103/PhysRevLett.89.117401